



CrossMark
click for updates

Cite this: *RSC Adv.*, 2016, 6, 50209

Received 13th February 2016
Accepted 5th May 2016

DOI: 10.1039/c6ra03955c

www.rsc.org/advances

Composition controlled nickel cobalt sulfide core-shell structures as high capacity and good rate-capability electrodes for hybrid supercapacitors†

Lei Zhang,‡ Haitao Zhang,‡* Long Jin, Binbin Zhang, Fangyan Liu, Hai Su, Fengjun Chun, Qinghan Li, Jinfang Peng and Weiqing Yang*

Herein, we report a type of core-shell structured $\text{Ni}_x\text{Co}_{3-x}\text{S}_4$ ($x = 1, 1.5$ and 2) through tuning the ratios of Ni to Co by a simple two-step hydrothermal method. Scanning electron microscopy and transmission electron microscopy images of all the Ni-Co sulfides show high porosity and uniform spherical morphology. Moreover, this study demonstrates that controlling the appropriate ratio of Ni to Co in the core-shell structure is crucial for improving the electrochemical performance in a hybrid supercapacitor. Among them, NiCo_2S_4 with core-shell structure possesses the highest capacity of 155 mA h g^{-1} , whereas as $\text{Ni}_{1.5}\text{Co}_{1.5}\text{S}_4$ shows the excellent rate-capability of up to 80% from 1 to 20 A g^{-1} and cycling stability, which retains 74% after 2000 cycles. Therefore, tuning the metal element contents provides

a feasible approach to achieving the desired high-rate performance and cycling stability of electrode materials in polynary metal sulfides for hybrid supercapacitors.

1. Introduction

With the depleting sources of fossil fuels available for the next century and the fast-growing use of electronics devices, exploring new energy sources and pursuing high performance energy-storage technologies are major challenges and are mandatory for the sustainable development of human civilization.¹⁻⁵ As two important types of electrochemical energy storage systems, lithium ion batteries (LIBs) and supercapacitors (SCs) are promising technological choices in virtue of the unique advantages of high round-trip efficiency, relatively high power density, and long cycling life.⁶⁻⁹ Herein, hybrid supercapacitors are a special type of capacitor system with similar electrochemical capacitor cells, which usually combines one battery-type electrode as an energy source with the other capacitive electrode as a power source.⁸ Therefore, just by means of these optimal qualities, many feasible and excellent applications, such as electric vehicles, high power portable devices, and backup energy systems, have been widely investigated.¹⁰⁻¹³ Among the abovementioned applications, the properties of the electroactive materials are vital to the performance of electrochemical energy storage systems.¹⁴⁻¹⁶

In the past few years, owing to the excellent electrochemical performance, transition metal sulfides, including binary and mixed-metal sulfides, have been intensively researched as desirable candidates for hybrid supercapacitors.¹⁷ Among these metal sulfides, to date, more considerable attention has been paid to ternary Ni-Co sulfides, because of their remarkable electrical conductivity, electrochemical activity and superior specific capacity, which are beneficial to electrochemical energy storage.¹⁸⁻²⁰ Recently, various nanostructures were prepared, such as ultrathin two-dimensional nanosheets,²¹ nanotubes,²² and hollow microspheres.²³⁻²⁶ By means of these unique nanostructures, high specific capacity, excellent rate capability and

Key Laboratory of Advanced Technologies of Materials (Ministry of Education), School of Materials Science and Engineering, Southwest Jiaotong University, Chengdu 610031, China. E-mail: wgyang@swjtu.edu.cn; haitaozhang@swjtu.edu.cn

† Electronic supplementary information (ESI) available: (1) The morphology of the precursor NiCo-glycerate spheres corresponding to the NiCo_2S_4 sample. (a and b) FESEM image. (c) TEM image. (2) SEM image and EDS-elemental mapping images of NiCo-glycerate spheres corresponding to the NiCo_2S_4 sample. (3) The SAED patterns of the Ni-Co sulfides: (a) NiCo_2S_4 , (b) $\text{Ni}_{1.5}\text{Co}_{1.5}\text{S}_4$, and (c) Ni_2CoS_4 . (4) SEM-EDS elemental mapping images and corresponding EDS spectra: (a) NiCo_2S_4 , (b) $\text{Ni}_{1.5}\text{Co}_{1.5}\text{S}_4$, and (c) Ni_2CoS_4 . (5) The ratio of nickel and cobalt according to their XPS data. (6) XRD patterns of the NiCo-glycerate precursor of NiCo_2S_4 , $\text{Ni}_{1.5}\text{Co}_{1.5}\text{S}_4$, and Ni_2CoS_4 . (7) The cyclic voltammetry curves with the scanning rate ranging from 2 to 100 mV s^{-1} of (a) NiCo_2S_4 , (b) $\text{Ni}_{1.5}\text{Co}_{1.5}\text{S}_4$, and (c) Ni_2CoS_4 . (8) The first six CV cycles at 0.5 mV s^{-1} of the (a) NiCo_2S_4 , (b) $\text{Ni}_{1.5}\text{Co}_{1.5}\text{S}_4$ and (c) Ni_2CoS_4 . Both samples are fully immersed in 6 M KOH solution overnight and tested with a fresh electrode, respectively. (9) The galvanostatic charging/discharging voltage profiles with the current density ranging from 1 to 20 A g^{-1} of (a) NiCo_2S_4 , (b) $\text{Ni}_{1.5}\text{Co}_{1.5}\text{S}_4$, and (c) Ni_2CoS_4 . (10) Rate capacity of Ni-Co sulfide with different micro/nano structures in three electrode configuration from recent reports. (11) The electrochemical impedance spectrum of (a) NiCo_2S_4 , (b) $\text{Ni}_{1.5}\text{Co}_{1.5}\text{S}_4$, and (c) Ni_2CoS_4 . (12) The 1st, 500th, 1000th, 1500th, 2000th charge and discharge cycles of (a) NiCo_2S_4 , (b) $\text{Ni}_{1.5}\text{Co}_{1.5}\text{S}_4$, and (c) Ni_2CoS_4 during 2000-cycle long-term cycling test. (13) XRD pattern of the nickel cobalt sulfides samples with nickel foam were characterized after 2000 cycles test in the ranges (a) 10–80° and (b) 24.5–40°. (14) FESEM images of the Ni-Co sulfides: (a and d) NiCo_2S_4 , (b and e) $\text{Ni}_{1.5}\text{Co}_{1.5}\text{S}_4$, and (c and f) Ni_2CoS_4 after cycling for 2000 cycles at a current density of 5 A g^{-1} . (15) CV curves of the nickel cobalt sulfides measured after 2000 charge and discharge cycles. See DOI: 10.1039/c6ra03955c

‡ These authors contributed equally to this work.

long cycle life were achieved, which implied that superior micro/nano structure design is crucial for improving the electrochemical performance.

Core-shell micro/nano-structures, as a unique family of functional materials with well-defined interior cores and functional shells, are of great interest. Their unique structural merits include large surface area, high pore volume, favourable stability, monodispersity and controllability, thus endowing them with the potential to be used in many fields, including catalysis,²⁷ sensors,²⁸ and energy conversion and storage systems,^{18,29} especially in terms of supercapacitors and lithium ion batteries. For instance, Y. Zhao *et al.* produced powdery carbon@MnO₂ core-shell hybrid spheres for electrochemical double layer supercapacitor electrode materials with a high specific capacitance of 252 F g⁻¹ at the scan rate of 2 mV s⁻¹ and 74% retention at 5 A g⁻¹ after 2000 cycles.³⁰ D. Cai *et al.* synthesized a ZnO@Co₃O₄ electrode that exhibited a high capacity of 166.7 mA h g⁻¹ at a current density of 1 A g⁻¹, which was higher than that of the Co₃O₄ electrode as well³¹ (note that the values of the battery-type electrodes based on the unit of F g⁻¹ were recalculated to mA h g⁻¹ for the purpose of this discussion). G. Zhang *et al.* synthesized carbon-coated CoMn₂O₄ core-shell spheres that present a high specific capacity of 726.7 mA h g⁻¹ with 1.0 M LiPF₆ in a 50 : 50 w/w mixture of ethylene carbonate and diethyl carbonate as the electrolyte.³² However, metal sulphides with these structures always undergo undesirable rate performance and poor cycling stability resulting from volumetric expansion and contraction of the electrode during the charging/discharging process.³³ As a result, much study has been performed to refine this capability, for instance, designing carefully complex structures^{18,34,35} and the composition of metal sulphides with carbonaceous materials.³⁶ Nevertheless, detailed investigations about the influence of controlling the content of nickel cobalt sulfides in various micro/nano structures on the electrochemical performance are rarely reported to date.³⁷

Herein, we report that the core-shell spheres Ni_xCo_{3-x}S₄ ($x = 1, 1.5$ and 2) have been prepared by a simple hydrothermal method through controlling the ratios of Ni to Co. These Ni-Co sulfide core-shell spheres with uniform spherical shape and high porosity show superior electrochemical properties. Furthermore, the specific capacity presents a decreasing trend with the increasing of cobalt content, and Ni_{1.5}Co_{1.5}S₄ exhibits excellent rate capability and superior cycle stability, which are crucial to electrochemical energy storage devices. Therefore, controlling the content of nickel and cobalt within core-shell micro/nano-structures can effectively achieve higher rate capability, cycling stability and superior battery-type performance of Ni-Co sulfide electroactive materials in hybrid supercapacitors.

2. Experimental

2.1 Synthesis of Ni_xCo_{3-x}S₄ core-shell spheres

All the chemicals were directly used as received without further purification. The process of preparing Ni_xCo_{3-x}S₄ core-shell spheres can be divided into two steps. First, in a typical synthesis procedure, 8 mL of glycerol and 40 mL of isopropanol

were mixed adequately. Subsequently, 0.125x mmol of Ni(NO₃)₂·6H₂O and 0.125(3 - x) mmol of Co(NO₃)₂·6H₂O were added to the abovementioned miscible liquids, where x was assigned as 1, 1.5, and 2 with a total of 0.375 mmol of nickel and cobalt. After stirring for about 20 min, a transparent pink solution was received and then transferred to a 100 mL Teflon-lined stainless steel autoclave and maintained at 180 °C for 6 h. The colour of the solution became weak gradually with the increase of nickel content. After cooling to ambient temperature naturally, the brown precipitate was collected by centrifugation, washed several times with ethanol and dried in an oven at 85 °C.

To prepare Ni_xCo_{3-x}S₄ core-shell spheres, 30 mg of the above-prepared NiCo-glycerate precursor and 50 mg of thioacetamide (TAA) were ultrasonically dispersed into 20 mL of ethanol. Then, the mixture was transferred to a 50 mL Teflon-lined stainless steel autoclave and maintained at 160 °C for 6 h. After being collected by centrifugation and washed with ethanol several times, the Ni_xCo_{3-x}S₄ core-shell spheres were obtained. Lastly, the final product was annealed under N₂ atmosphere at 300 °C for 40 min to improve the crystallinity.

2.2 Materials characterization

The morphology and structure were characterized by using field-emission scanning electron microscopy (FESEM) (JEOL, JSM-7001F). SEM elemental mapping was acquired by using an energy-dispersive X-ray spectrometer (EDS) attached to a JSM-7100F. Samples were dispersed over a silicon substrate for SEM and EDS characterizations. Transmission electron microscopy (TEM) and high-resolution TEM (HRTEM) characterizations were performed with a JEOL JEM-2100F operating at an accelerating voltage of 200 kV. STEM elemental mapping was acquired by using the EDS attached to a JEM-2100F. X-ray diffraction (XRD) patterns were performed with an X'Pert Pro MPD (Holland) X-ray diffractometer with Cu K α 1 radiation ($\lambda = 0.154$ nm) between 10° and 80°. X-ray photoelectron spectroscopy (XPS) characterizations were performed with a Kratos XSAM800 spectrometer.

2.3 Electrochemical measurements

For characterizing electrochemical performance, the measuring electrodes were prepared by mixing the electroactive material, acetylene black and polyfluortetraethylene (PTFE) binder in a weight ratio of 85 : 8 : 7 in isopropyl alcohol, and the mixture was blended for 30 min before using. The obtained slurry was dripped onto Ni foam (about 500 μ m) with a loading area of 1 cm². The loading mass of materials in each electrode was about 1–2 mg, controlled carefully based on the Mettler Toledo MS105DU electronic balance with the precision of 0.01 mg. Last, this abovementioned nickel foam was rolled down to 100–120 μ m thick films and dried at 85 °C for 12 h to remove excess isopropanol. Then, a CHI660E electrochemical workstation (Shanghai Chenhua Instrument Co. Shanghai, China) was utilized for electrochemical measurements with a 6.0 M aqueous KOH electrolyte in a three-electrode configuration, wherein a Pt foil with an area of 3 cm \times 2 cm served as the counter electrode and an Hg/HgO electrode as the reference

electrode. Finally, a LAND battery test system was used for long cycle life measurements by a chronopotentiometry technique. The specific capacity was calculated by the following equation:

$$C = \frac{I\Delta t}{m} \quad (1)$$

where C is the specific capacity with units of mA h g^{-1} , I is the discharge current with units of mA , Δt is the discharge time with units of hours (h), and m is the mass of the active material with units of grams (g).

3. Results and discussion

The composition controlled $\text{Ni}_x\text{Co}_{3-x}\text{S}_4$ ($x = 1, 1.5$ and 2) were prepared by a two-step hydrothermal method. First, just as shown in Fig. S1,† the precursors, nickel cobalt glycerate (NiCo-glycerate), were prepared with morphology of highly consistent solid spheres. Furthermore, the EDS-mapping images of these precursors also show well-proportioned typical metal alkoxides (Fig. S2†). Subsequently, a typical hydrothermal anion-exchange sulfidation process,¹⁸ as presented in Fig. 1a, was then utilized to convert the NiCo-glycerate solid spheres into core-shell

$\text{Ni}_x\text{Co}_{3-x}\text{S}_4$ hollow spheres. In particular, the decomposition of thioacetamide (TAA) at a high temperature makes S^{2-} react with the surface of NiCo-glycerate solid spheres at stage I. This sulfidation process can be expressed as an anion exchange reaction/micro-level Kirkendall effect of the NiCo-glycerate. At stage II, the well-defined core-shell structure was gradually formed as a result of the different diffusion rates between faster outward metal ions (Ni^{2+} , Co^{2+}) and inward sulfur ions. When the gap between the core and shell enlarge to a certain degree, it becomes more difficult for the metal ions to diffuse to the shell. Moreover, a similar anion exchange reaction occurs in the cores. Thus, the uniform composition controlled nickel cobalt sulfides were obtained with the completion of the reaction at stage III. The detailed synthesis procedure has been presented in the Method section.

The morphology and nanostructure of the as-synthesized nickel cobalt sulfides were characterized by field emission scanning electron microscopy (FESEM) and transmission electron microscopy (TEM). Despite having different Ni-Co molar ratios, these low-magnification FESEM images demonstrate that the nickel cobalt sulfides are quite similar in morphology and structure, as presented in Fig. 1b-d. All the samples are

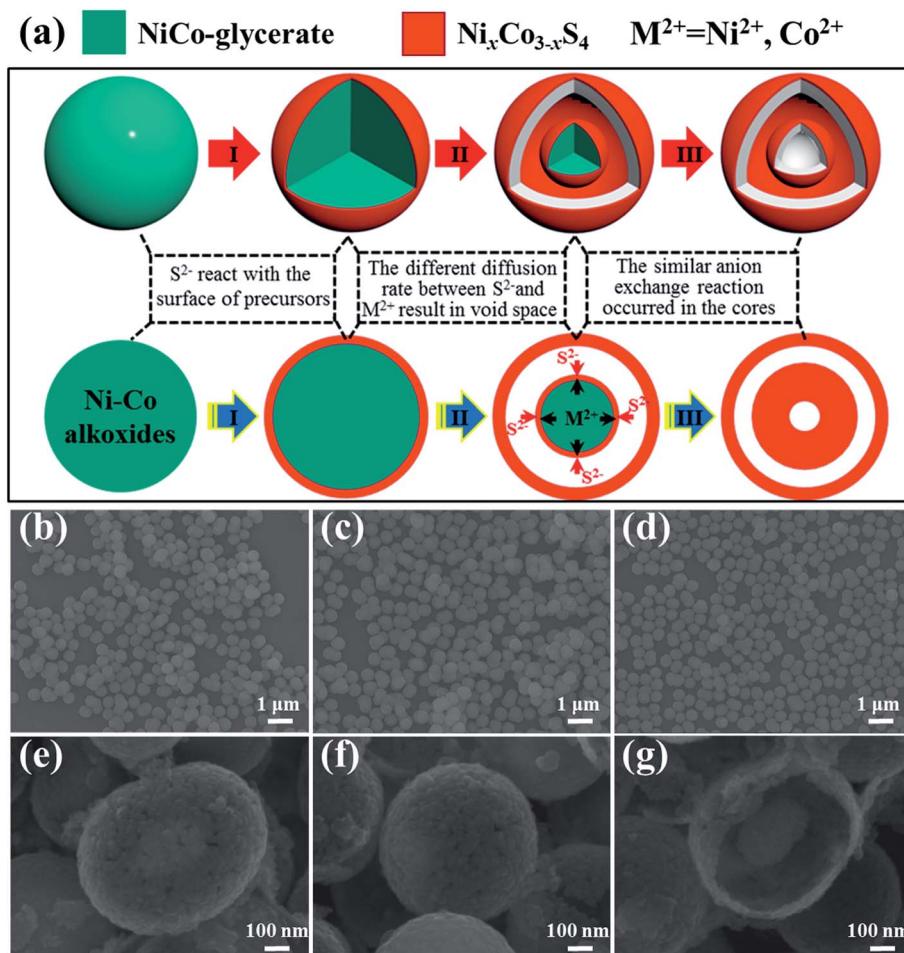


Fig. 1 (a) Schematic of the formation process of core-shell nickel cobalt spheres with a series of 3D and 2D images. (b-d) SEM images of the Ni-Co sulfides: NiCo_2S_4 , $\text{Ni}_{1.5}\text{Co}_{1.5}\text{S}_4$, and Ni_2CoS_4 , respectively. (e-g) Enlarged SEM images.

composed of uniform well-dispersed spheres in accord with the precursors. The surfaces of the samples mentioned above were rough and porous not only in the shell, but also in the core (Fig. 1g), which implied a high specific surface area and much more effective ion/electron transfer channels.

The detailed morphology and interior structural features of the corresponding samples were further investigated by TEM characterizations, as shown in Fig. 2a–c. The similar morphology and structure of the nickel cobalt sulfides are consistent with the SEM measurements. Interestingly, there are many mesopores on the surface of the resulted samples displayed in Fig. 2d–f. The lattice spacing of NiCo_2S_4 are observed to be 0.18 nm and 0.28 nm in the HRTEM images, as shown in Fig. 2g, which are in good agreement with the interplanar spacing of NiCo_2S_4 (511) and (311) planes.³⁸ Apart from this, the counterpart of Ni_2CoS_4 is 0.23 nm, as presented in Fig. 2i, corresponding to the interplanar spacing of (400) planes.³⁹ In addition, the lattice spacing of 0.33 nm (Fig. 2h) in the $\text{Ni}_{1.5}\text{Co}_{1.5}\text{S}_4$ sample should belong to the interplanar spacing of (220) planes, which is similar to its counterpart 0.332 nm in NiCo_2S_4 and 0.334 nm in Ni_2CoS_4 .^{38,39} To further investigate the crystalline phase and the purity of the Ni–Co sulfides, the selected area electron diffraction (SAED) results were obtained and displayed in Fig. S3.† The diffraction rings can be assigned to the (440), (511), (400), (311), and (220) planes of the NiCo_2S_4 phase.³⁸ The well-defined diffraction rings of all the nickel cobalt sulfide patterns demonstrate the polycrystalline nature of all the samples. Although the SAED patterns result from their high similarity in crystal structure, the value of the diameter of these diffraction rings become smaller with the increase of cobalt content, which is consistent with the results of HRTEM.

Energy-dispersive X-ray spectroscopy (EDS) elemental mapping analysis was exhibited in Fig. 3a–c. It unambiguously proves that the composition controlled NiCo_2S_4 , $\text{Ni}_{1.5}\text{Co}_{1.5}\text{S}_4$

and Ni_2CoS_4 core-shell spheres were successfully prepared. Obviously, the distributions of Ni, Co and S elements in these core-shell spheres are uniform, which certify the coexistence of the nickel and cobalt ions in the core-shell $\text{Ni}_x\text{Co}_{3-x}\text{S}_4$ samples. The right-hand inset presents the detailed elemental ratio of NiCo_2S_4 , $\text{Ni}_{1.5}\text{Co}_{1.5}\text{S}_4$ and Ni_2CoS_4 with the similar Ni–Co element ratio of 1 : 2, 1 : 1, and 2 : 1, respectively. In addition, the extensive elemental mapping analysis was carried out by SEM, as presented in Fig. S4.† Note that the highest element peak can be ascribed to the silicon element because the samples were dispersed onto a silicon substrate for EDS detections. Apart from this, X-ray photoelectron spectroscopy (XPS) was utilized to determine clearly the chemical state of the Ni and Co elements of the core-shell Ni–Co sulfide samples. The deconvoluted peaks of Ni 2p and Co 2p were shown in Fig. 3d. The Ni 2p doublets display the atoms located at 856.6 eV (Ni^{2+}) and 861 eV (Ni^{3+}) in $2p_{3/2}$ and 874.8 eV (Ni^{2+}) and 879.3 eV (Ni^{3+}) in $2p_{1/2}$. Similarly, the corresponding Co 2p peaks show electronic configurations at 797.3 eV (Co^{2+}) and 793 eV (Co^{3+}) in $2p_{1/2}$ and 781.3 eV (Co^{2+}) and 777.9 eV (Co^{3+}) in $2p_{3/2}$. In addition, two satellite peaks were observed in each high-resolution Ni 2p and Co 2p spectra. Moreover, the ratios of nickel and cobalt are about 1 : 1.9, 1 : 1.1, and 1.9 : 1 for the NiCo_2S_4 , $\text{Ni}_{1.5}\text{Co}_{1.5}\text{S}_4$, and Ni_2CoS_4 samples, respectively, according to their XPS data (Table S1†).

The nickel cobalt sulfide powder XRD patterns were depicted in Fig. 4. Compared with the XRD pattern of solid sphere NiCo-glycerates (Fig. S5†), the as-grown core-shell hollow sphere $\text{Ni}_x\text{Co}_{3-x}\text{S}_4$ have good crystallinity, mainly ascribing to the annealing process under the N_2 atmosphere at 300 °C. All the diffraction peaks of the NiCo_2S_4 , $\text{Ni}_{1.5}\text{Co}_{1.5}\text{S}_4$, and Ni_2CoS_4 samples reveal their relatively good crystallinity. For NiCo_2S_4 , the overall Bragg peaks can be indexed to the cubic NiCo_2S_4 phase (JCPDS card 20-0782). With the change of the nickel and

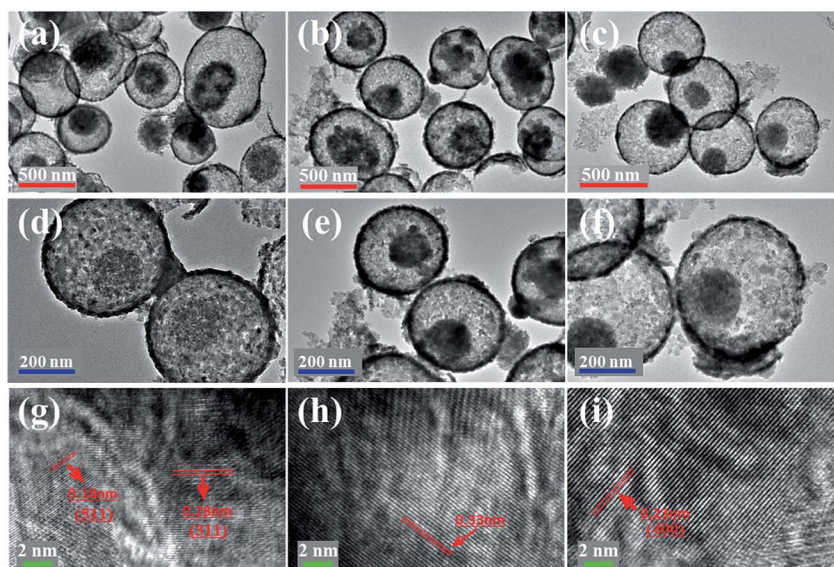


Fig. 2 TEM images of the Ni–Co sulfides: (a and d) NiCo_2S_4 , (b and e) $\text{Ni}_{1.5}\text{Co}_{1.5}\text{S}_4$, and (c and f) Ni_2CoS_4 , respectively. (g–i) Corresponding HRTEM images.

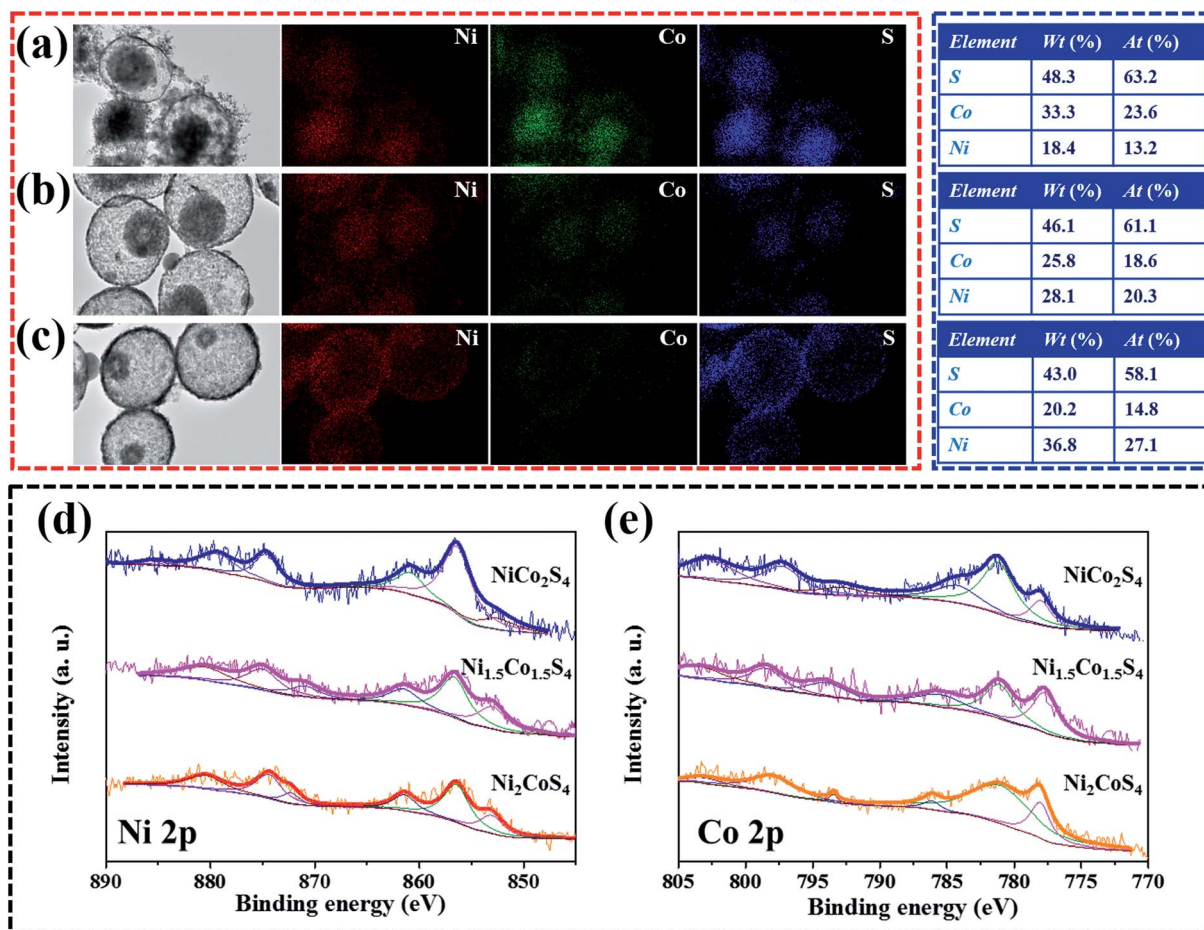


Fig. 3 STEM-EDS elemental mapping images of (a) NiCo_2S_4 , (b) $\text{Ni}_{1.5}\text{Co}_{1.5}\text{S}_4$, and (c) Ni_2CoS_4 . Inset: the corresponding EDS spectrum. XPS spectra of all the nickel cobalt sulfides: (d) Ni 2p, (e) Co 2p.

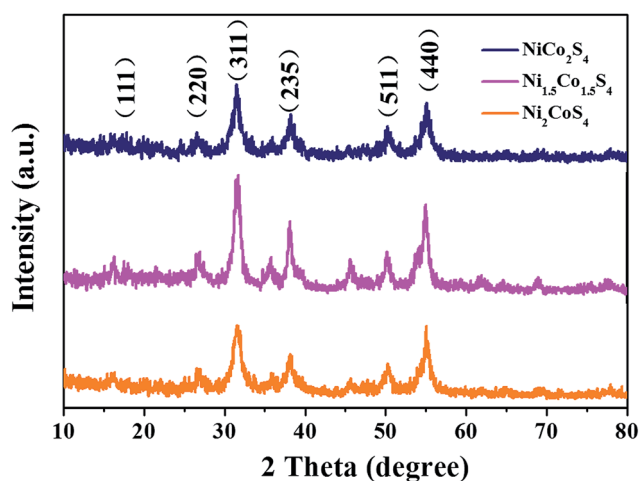
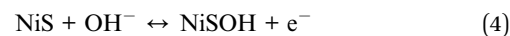
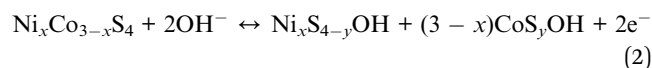


Fig. 4 XRD patterns of NiCo_2S_4 , $\text{Ni}_{1.5}\text{Co}_{1.5}\text{S}_4$, and Ni_2CoS_4 .

cobalt molar ratio, all the diffraction peaks of the samples moved towards the low angle direction, owing to the bigger lattice parameter of the Co element. The size of the cubic crystal structure gradually increases from Ni_2CoS_4 to NiCo_2S_4 , which further validates the results of HRTEM and SAED.^{38,39}

The electrochemical properties of the core-shell nickel cobalt sulfides are shown in Fig. 5. The representative cyclic voltammetry (CV) curves of NiCo_2S_4 , $\text{Ni}_{1.5}\text{Co}_{1.5}\text{S}_4$, and Ni_2CoS_4 in a potential window ranging from -0.1 to 0.55 V at a scan rate of 5 mV s^{-1} are displayed in Fig. 5a. Apparently, a pair of redox peaks can be observed in the CV curves, indicating the faradaic nature of the nickel cobalt sulfides in the electrochemical process. The redox peaks can be attributed to redox reactions as follows:^{18,37}



where in eqn (2), $x = 1, 1.5, 2$. The detailed CV curves at various scan rates ranging from 2 to 100 mV s^{-1} for NiCo_2S_4 , $\text{Ni}_{1.5}\text{Co}_{1.5}\text{S}_4$, and Ni_2CoS_4 electrodes were displayed in Fig. S6.† There are no distinct changes in the position and shape of the current peaks, demonstrating that the nickel cobalt sulfide electrodes are capable of fast redox reactions. These distinct redox peaks in the CV curves of all the samples may be

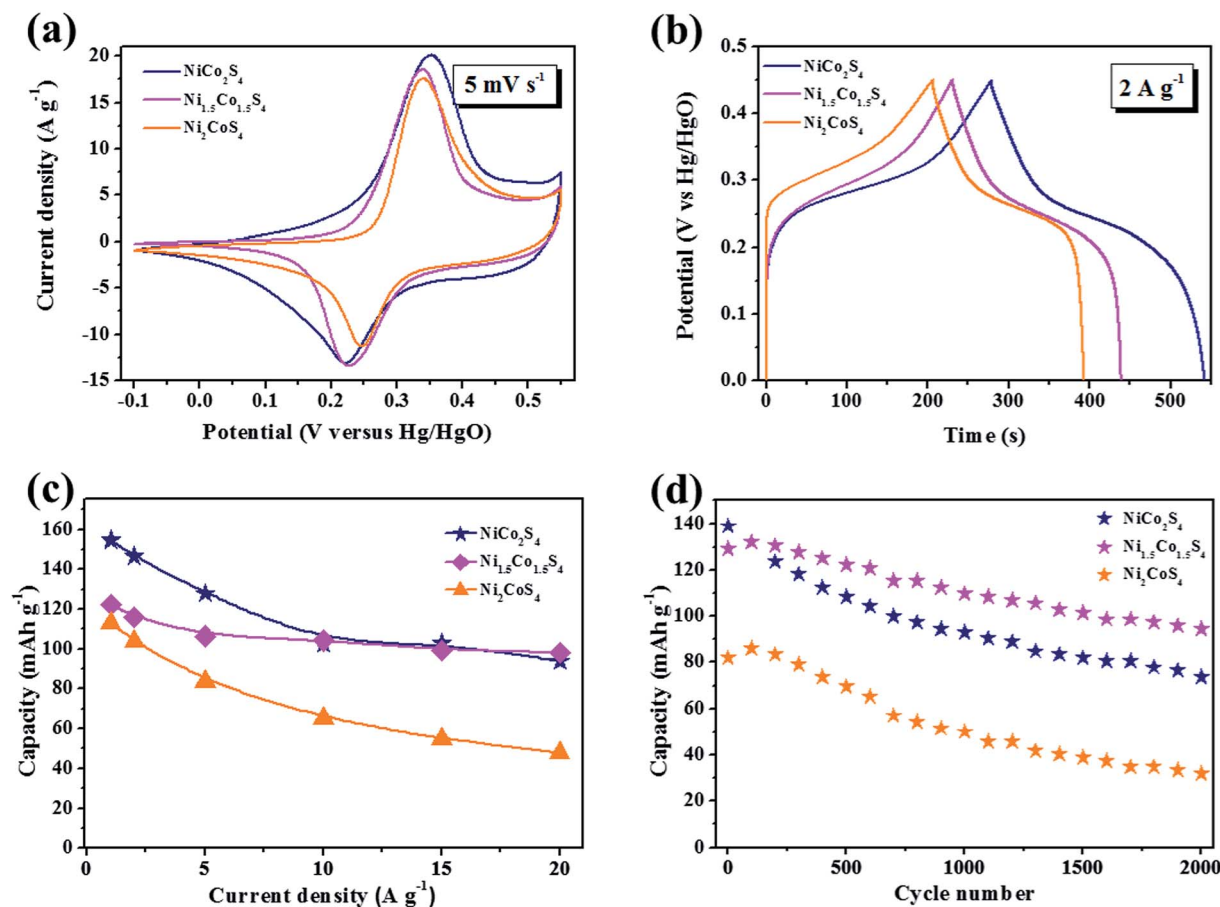


Fig. 5 Electrochemical evaluations of the nickel cobalt sulfides: (a) cyclic voltammograms at 5 mV s^{-1} , (b) galvanostatic charging/discharge voltage curves at 2 A g^{-1} , (c) specific capacity with different current densities ranging from 1 to 20 A g^{-1} and (d) the cycling lifetime at a discharge current density of 5 A g^{-1} .

attributed to the redox reaction of $\text{Ni}^{2+}/\text{Ni}^{3+}$ and $\text{Co}^{2+}/\text{Co}^{4+}$.³⁷ Just as shown in Fig. S7,† the fresh electrodes of all the nickel cobalt sulfides were used for the CV test after immersing in 6 M KOH solution overnight with a low scan rate at 0.5 mV s^{-1} . Though we observed an obvious anodic peak corresponding to the redox reaction of $\text{Co}^{2+}/\text{Co}^{3+}$ in the first three cycles, the redox reaction of $\text{Co}^{2+}/\text{Co}^{3+}$ seems to be irreversible, as demonstrated by the absence of the reduction peak.

Fig. 5b presents the galvanostatic charge/discharge (GCD) curves of the nickel cobalt sulfide electrodes at different time intervals at a current density of 2 A g^{-1} . The theoretical value (C_T) of the electrode materials can be calculated by the following equation:

$$C_T = (n \times F)/(M \times 3.6) \quad (5)$$

where n is the number of electrons transferred in the electrochemical process, F is the Faraday constant, and M is the molar mass of the electrode material. Owing to the molar mass of Ni and Co being almost the same, the difference in the theoretical capacity of Ni and Co ions is mainly attributed to the number of electrons transferred in the redox reaction. In theory, only one electron was converted from every Ni^{2+} to Ni^{3+} ($n = 1$). However,

two electrons were oxidized, from every Co^{2+} to Co^{4+} ($n = 2$). According to eqn (5), the theoretical capacity of Co-based compounds is much higher than that of the corresponding Ni-based compounds. Thus, just as shown in Fig. 5b, as the Co content increases, the experimental specific capacity of nickel cobalt sulfides maintain an increasing trend with the values of 155, 122, and 113 mA h g^{-1} . The detailed GCD curves of the nickel cobalt sulfides with a different Ni-Co ratio were displayed in Fig. S8† at various current densities ranging from 1 to 20 A g^{-1} . Compared with other micro/nano structures, the core-shell spheres present an excellent electrochemical performance. For example, Y. Zhu *et al.* prepared an acetylene black decorated NiCo_2S_4 hollow microsphere with a specific capacity of 117 mA h g^{-1} at 2 A g^{-1} .^{23,39} Y. Chen *et al.* synthesized uniform one-dimensional nickel cobalt sulfide hollow tubular structures with a specific capacity of 150 mA h g^{-1} at 2 A g^{-1} .^{21,40} Z. Wu *et al.* produced high-purity NiCo_2S_4 mesoporous nanosheets with a specific capacity of 124 mA h g^{-1} at 1 A g^{-1} .⁴¹ More importantly, this is the first investigation to tune the capability of the nickel cobalt sulfides with a core-shell structure. It is apparent that controlling the content of Co ions and Ni ions is effective in tuning the capacitive performance for core-shell structured nickel cobalt sulfides.

Subsequently, the specific capacity of the nickel cobalt sulfides at different current densities were calculated based on the GCD measurements and the results were shown in Fig. 5c. While the specific capacity of the Ni–Co sulfide electrodes gradually decreases with the increase of current density, the specific capacity still maintains high values of 94, 98, and 48 mA h g⁻¹, corresponding to NiCo₂S₄, Ni_{1.5}Co_{1.5}S₄, and Ni₂CoS₄. After a 20-fold increase in current density, the capacity retentions of the NiCo₂S₄, Ni_{1.5}Co_{1.5}S₄, and Ni₂CoS₄ are 61%, 80%, and 42%, respectively. The Ni_{1.5}Co_{1.5}S₄ exhibits the highest rate capacity up to 80% at all measured current densities compared to NiCo₂S₄ and Ni₂CoS₄. In addition, it is worth noting that the Ni_{1.5}Co_{1.5}S₄ core–shell spheres present the excellent rate capacity among various micro/nano structures from recently reported of the nickel cobalt sulfides, which was indexed in Table S2.† The electrochemical impedance spectroscopy (EIS) plots of the Ni–Co sulfides were shown in Fig. S9.† Ni_{1.5}Co_{1.5}S₄ presents the smallest resistance and the slope in the low frequency region indicates fast transfer of electrons in the charge–discharge process and a better rate capability. The EIS plots are fitted based on the equivalent circuit model and exhibited in the inset.

Cycling performance, as another important factor for supercapacitor applications, was calculated from results of the GCD test at a current density of 5 A g⁻¹, as presented in Fig. 5d. The specific capacities are 139, 129, and 82 mA h g⁻¹ for the first cycle and the values decrease to 74, 95, and 32 mA h g⁻¹ for NiCo₂S₄, Ni_{1.5}Co_{1.5}S₄, and Ni₂CoS₄, respectively, which corresponds to 53%, 74%, and 40% retainment after continuous cycling for 2000 cycles and proves that tuning the metal element content in polynary metal sulfides can be a feasible approach by which to obtain the desired high rate performance and cycling stability electrode materials. The 1st, 500th, 1000th, 1500th, and 2000th charge and discharge cycles of NiCo₂S₄, Ni_{1.5}Co_{1.5}S₄, and Ni₂CoS₄ during the 2000-cycle long-term cycling test was illustrated in Fig. S10.† After 2000 charge–discharge cycles, the NiCo₂S₄, Ni_{1.5}Co_{1.5}S₄, and Ni₂CoS₄ samples were each characterized to demonstrate the evolution of the Ni–Co sulfides during the long-cycling test. Fig. S11† shows the XRD patterns of the nickel cobalt sulfides after 2000 cycles. It demonstrates that some of the nickel cobalt sulfides were decomposed, which may be ascribed to the volume effect induced by ion/electron transport kinetics.³³ We further detected that the samples were composed of some nanosheets after the cycling test. Moreover, the CV curves after 2000 cycles (Fig. S13†) present two redox peaks, which further indicates this result. Thus, we suggest that the cycling stability of the polynary metal sulfides can be further improved by a strategy of inhibiting the decomposition of these materials.

4. Conclusions

In summary, a series of core–shell Ni–Co sulfides with different Ni and Co contents have been prepared by a simple two-step hydrothermal method. From the electrochemical measurements for these bimetallic nickel cobalt sulfides with a core–shell structure, NiCo₂S₄ possesses the superior specific capacity of 155

mA h g⁻¹ at 1 A g⁻¹, but Ni_{1.5}Co_{1.5}S₄ performs more excellently in rate capability, *i.e.*, 80% capacity retention from 1 to 20 A g⁻¹, and long cycle stability (74% after 2000 cycles). This study demonstrates that in the polynary metal sulfides, the appropriate content of nickel and cobalt ions in the core–shell structure are crucial for superior electrochemical performance. Therefore, optimizing their electrochemical performance for hybrid supercapacitors by tuning the content of every component in polynary electrode materials is attainable.

Conflict of interest

The authors declare no competing financial interest.

Acknowledgements

This study is supported by the scientific and technological projects for distinguished young scholars of China (No. 2015JQ0013) and the Fundamental Research Funds for the Central Universities of China (A0920502051408).

References

- 1 J. Chen, G. Zhu, W. Yang, Q. Jing, P. Bai, Y. Yang, T. C. Hou and Z. L. Wang, *Adv. Mater.*, 2013, **25**, 6094–6099.
- 2 W. Yang, J. Chen, G. Zhu, X. Wen, P. Bai, Y. Su, Y. Lin and Z. Wang, *Nano Res.*, 2013, **6**, 880–886.
- 3 W. Yang, J. Chen, Q. Jing, J. Yang, X. Wen, Y. Su, G. Zhu, P. Bai and Z. L. Wang, *Adv. Funct. Mater.*, 2014, **24**, 4090–4096.
- 4 H. T. Zhang, X. Zhang, X. Z. Sun, D. C. Zhang, H. Lin, C. H. Wang, H. J. Wang and Y. W. Ma, *ChemSusChem*, 2013, **6**, 1084–1090.
- 5 L. Zhang, B. Zhang, J. Chen, L. Jin, W. Deng, J. Tang, H. Zhang, H. Pan, M. Zhu, W. Yang and Z. L. Wang, *Adv. Mater.*, 2016, **28**, 1650–1656.
- 6 P. Simon and Y. Gogotsi, *Nat. Mater.*, 2008, **7**, 845–854.
- 7 J. R. Miller and P. Simon, *Science*, 2008, **321**, 651–652.
- 8 T. Brousse, D. Belanger and J. W. Long, *J. Electrochem. Soc.*, 2015, **162**, A5185–A5189.
- 9 H. Zhang, X. Sun, X. Zhang, H. Lin, K. Wang and Y. Ma, *J. Alloys Compd.*, 2015, **622**, 783–788.
- 10 B. Conway, *Electrochemical supercapacitors: scientific fundamentals and technological applications*, Academic, Plenum Publishers: Kluwer, New York, 1st edn, 1999.
- 11 G. P. Wang, L. Zhang and J. J. Zhang, *Chem. Soc. Rev.*, 2012, **41**, 797–828.
- 12 T. W. Lin, M. C. Hsiao, S. W. Chou, H. H. Shen and J. Y. Lin, *J. Electrochem. Soc.*, 2015, **162**, A1493–A1499.
- 13 H. Zhang, L. Zhang, J. Chen, H. Su, F. Liu and W. Yang, *J. Power Sources*, 2016, **315**, 120–126.
- 14 H. Zhang, X. Zhang, X. Sun and Y. Ma, *Sci. Rep.*, 2013, **3**, 3534.
- 15 H. Zhang, X. Zhang and Y. Ma, *Electrochim. Acta*, 2015, **184**, 347–355.
- 16 H. Zhang, K. Wang, X. Zhang, H. Lin, X. Sun, C. Li and Y. Ma, *J. Mater. Chem. A*, 2015, **3**, 11277–11286.

- 17 K. Krishnamoorthy, G. Veerasubramani, P. Pazhamalai and S. J. Kim, *Electrochim. Acta*, 2015, **190**, 305–312.
- 18 L. F. Shen, L. Yu, H. B. Wu, X. Y. Yu, X. G. Zhang and X. W. Lou, *Nat. Commun.*, 2015, **6**, 6694.
- 19 C. Xia, P. Li, A. N. Gandi, U. Schwingenschlöggl and H. N. Alshareef, *Chem. Mater.*, 2015, **27**, 6482–6485.
- 20 L. Yu, L. Zhang, H. B. Wu and X. W. Lou, *Angew. Chem., Int. Ed.*, 2014, **53**, 3711–3714.
- 21 X. Li, Q. Li, Y. Wu, M. Rui and H. Zeng, *ACS Appl. Mater. Interfaces*, 2015, **7**, 19316–19323.
- 22 Z. Yang, X. Zhu, K. Wang, G. Ma, H. Cheng and F. Xu, *Appl. Surf. Sci.*, 2015, **347**, 690–695.
- 23 Y. Zhu, X. Ji, Z. Wu and Y. Liu, *Electrochim. Acta*, 2015, **186**, 562–571.
- 24 J. Xiao, L. Wan, S. Yang, F. Xiao and S. Wang, *Nano Lett.*, 2014, **14**, 831–838.
- 25 K. Xu, W. Li, Q. Liu, B. Li, X. Liu, L. An, Z. Chen, R. Zou and J. Hu, *J. Mater. Chem. A*, 2014, **2**, 4795.
- 26 Y. Xiao, D. Su, X. Wang, L. Zhou, S. Wu, F. Li and S. Fang, *Electrochim. Acta*, 2015, **176**, 44–50.
- 27 J. L. Li, X. J. Liu, X. Q. Piao, Z. Sun and L. K. Pan, *RSC Adv.*, 2015, **5**, 16592–16597.
- 28 M. Liu, Z. Y. Wang, S. F. Zong, H. Chen, D. Zhu, L. Wu, G. H. Hu and Y. P. Cui, *ACS Appl. Mater. Interfaces*, 2014, **6**, 7371–7379.
- 29 J. Zang, J. J. Chen, C. L. Zhang, H. Qian, M. S. Zheng and Q. F. Dong, *J. Mater. Chem. A*, 2014, **2**, 6343–6347.
- 30 Z. Yong, Y. Meng and J. Peng, *J. Power Sources*, 2014, **259**, 219–226.
- 31 D. P. Cai, H. Huang, D. D. Wang, B. Liu, L. L. Wang, Y. Liu, Q. H. Li and T. H. Wang, *ACS Appl. Mater. Interfaces*, 2014, **6**, 15905–15912.
- 32 G. Q. Zhang and X. W. Lou, *Angew. Chem., Int. Ed.*, 2014, **53**, 9041–9044.
- 33 X.-Y. Yu, L. Yu and X. W. D. Lou, *Adv. Energy Mater.*, 2016, **6**, 1501333.
- 34 X. Y. Yu, L. Yu, B. H. Wu and X. W. Lou, *Angew. Chem., Int. Ed.*, 2015, **54**, 5331–5335.
- 35 L. Zhang, H. B. Wu, Y. Yan, X. Wang and X. W. Lou, *Energy Environ. Sci.*, 2014, **7**, 3302–3306.
- 36 H. Hu, L. Han, M. Z. Yu, Z. Y. Wang and X. W. Lou, *Energy Environ. Sci.*, 2016, **9**, 107–111.
- 37 H. C. Chen, J. J. Jiang, Y. D. Zhao, L. Zhang, D. Q. Guo and D. D. Xia, *J. Mater. Chem. A*, 2015, **3**, 428–437.
- 38 S. Bowie, *Econ. Geol.*, 1967, **62**, 278–282.
- 39 C.-H. Huang and O. Knop, *Can. J. Chem.*, 1971, **49**, 598–602.
- 40 Y. M. Chen, Z. Li and X. W. Lou, *Angew. Chem., Int. Ed.*, 2015, **54**, 10521–10524.
- 41 Z. Wu, X. Pu, X. Ji, Y. Zhu, M. Jing, Q. Chen and F. Jiao, *Electrochim. Acta*, 2015, **174**, 238–245.